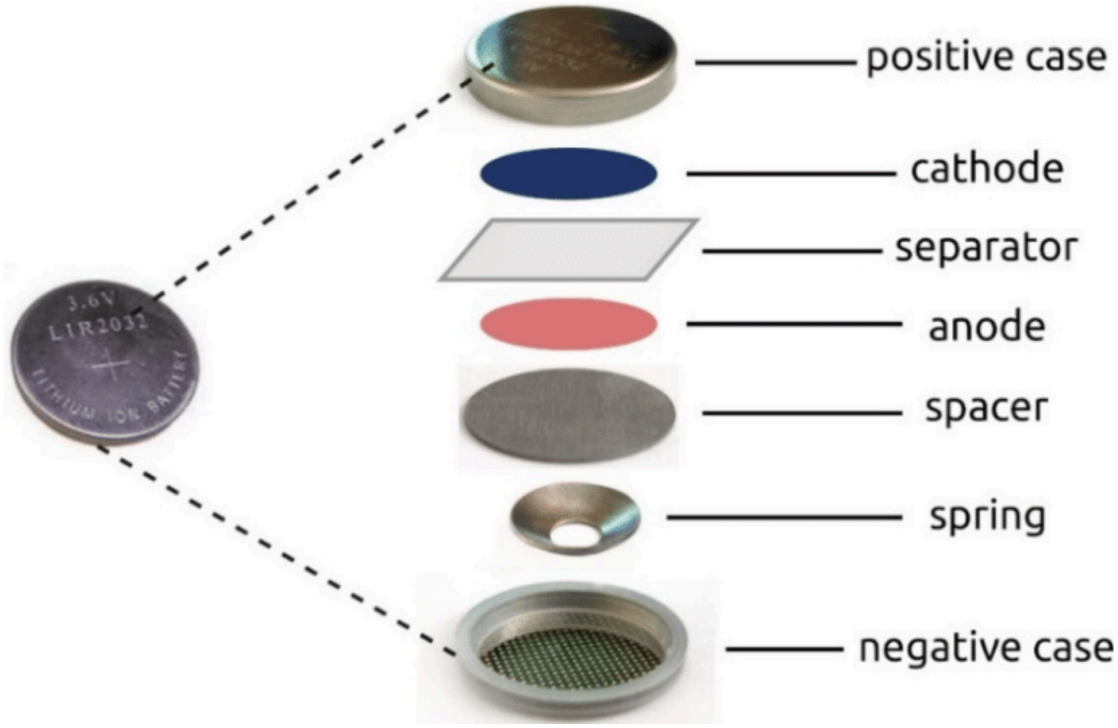

Impact of Cathode Materials, Thickness, and Charging C-rate on Lithium Deposition in Lithium-Ion Batteries

Master's Thesis in Electrical engineering

Zhen Chang

DEPARTMENT OF ELECTRICAL ENGINEERING

CHALMERS UNIVERSITY OF TECHNOLOGY
Gothenburg, Sweden 2025
www.chalmers.se

Master's Thesis 2025

Impact of Cathode Materials, Thickness, and Charging C-rate on Lithium Deposition in Lithium-Ion Batteries

ZHEN CHANG

CHALMERS
UNIVERSITY OF TECHNOLOGY

Department of Electrical Engineering
Division of Sustainable Electric Power Engineering and Electromobility
Chalmers University of Technology
Gothenburg, Sweden 2025

Impact of Cathode Materials, Thickness, and Charging C-rate on Lithium Deposition in Lithium-Ion Batteries

Supervisor: YUJING LIU, Sustainable electric power engineering and electromobility
Examiner:YUJING LIU, Sustainable electric power engineering and electromobility

Master's Thesis 2025
Department of Electrical Engineering
Division of Sustainable Electric Power Engineering and Electromobility

Chalmers University of Technology
SE-412 96 Gothenburg
Telephone +46 31 772 1000

Cover: Lithium-Ion Batteries Coin cell.

Printed by Chalmers Reproservice
Gothenburg Sweden 2025

Impact of Cathode Materials, Thickness, and Charging C-rate on Lithium Deposition in Lithium-Ion Batteries

ZHEN CHANG
Department of Electrical Engineering
Chalmers University of Technology

Abstract

Lithium-ion batteries (LIBs) are widely used in modern energy storage systems due to their high energy density, long cycle life, and fast charging capability. However, lithium plating during high-rate charging remains a critical challenge, leading to capacity degradation, impedance rise, and safety risks such as internal short circuits and thermal runaway.

This thesis investigates how cathode material properties, electrode thickness, and charging protocols collectively influence lithium plating and capacity loss in coin cells paired with lithium metal-based anodes. Three cathode chemistries are examined: NMC811 (Nickel Manganese Cobalt), LFP (Lithium Iron Phosphate), and LFMP (Lithium Manganese Iron Phosphate). Galvanostatic cycling was performed under stepwise increasing C-rates (0.1C, 1C, 2C) to evaluate capacity retention and CE behavior. Electrochemical Impedance Spectroscopy (EIS) was conducted after all cycling was completed, to assess the cumulative development of internal resistance and interfacial degradation.

The results show that cathode composition significantly affects interfacial stability. NMC811 exhibits the highest initial capacity but suffers from rapid impedance growth at high rates. LFP shows superior cycling stability and minimal impedance change, while LFMP offers intermediate performance but is sensitive to abrupt fast charging. Thicker electrodes tend to accelerate capacity fade due to transport limitations, whereas thinner ones provide more stable cycling behavior. Moreover, stepwise charging protocols improve efficiency across all systems, particularly mitigating degradation in LFMP cells.Overall, this work provides insights into the interplay between material selection, electrode design, and fast-charging strategies, offering guidance for improving the performance and reliability of lithium-ion batteries in high-rate applications.

Keywords: Lithium plating, Electrode thickness, Fast charging, Lithium-ion battery, Impedance spectroscopy

Acknowledgements

I would like to sincerely thank my supervisor and examiner, Professor Yujing Liu, for his invaluable guidance and timely support throughout my thesis work. His mentorship significantly accelerated my learning and enabled me to contribute more effectively to the research.

I am also deeply grateful to my co-supervisor, Dr. Zhe Qu, for her consistent guidance and support on both the experimental work and the writing of this thesis.

My heartfelt gratitude goes to my family and friends for their unwavering support, encouragement, and care throughout this journey. Lastly, I extend my sincere appreciation to everyone who has inspired me to think critically and explore new perspectives.

Lastly, I extend my sincere appreciation to everyone who has inspired me to think critically and explore new perspectives.

Zhen Chang , Gothenburg, April 2025

List of Acronyms

Below is the list of acronyms that have been used throughout this thesis listed in alphabetical order:

BES	Battery Energy Storage
RES	Renewable-based Energy Sources
R_{ct}	Charge transfer resistance
R_{l}	Long time transient resistance
Ω	Ohmic resistance
R_{SEI}	Resistance of the surface film layer on the electrodes
R_{s}	Short time transient resistance
Z_{exp}	Warburgs impedance
Zexp	Measured impedance
Z_{sim}	Simulated impedance
W	Warburg
Q	Constant Phase Element
R	Resistance
AC	Alternating Current
BEV	Battery Electric Vehicle
PVDF	polyvinylidene fluoride
CC	Constant current charge or discharge
CPE	Constant Phase Element
CV	Constant voltage charge or discharge
DC	Direct Current
EIS	Electrochemical Impedance Spectroscopy
EoL	End of Life
LFP	LiFePO4; Lithium Iron Phosphate
NMC811	Nickel Manganese Cobalt
LFMP	Lithium Man- ganese Iron Phosphat
OCV	Open Circuit Voltage
PHEV	Plug-in Hybrid Electric Vehicle
SEI	Solid Electrolyte Interphase
SoC	State of Charge

Nomenclature

Below is the nomenclature of indices, sets, parameters, and variables that have been used throughout this thesis.

Indices

t	Index for time step

Sets

Parameters

Variables

V_{charge}	The cell voltage measured during the charging process
$V_{discharge}$	The cell voltage measured during the discharging process

Contents

List of Figures

List of Tables

1

Introduction

1.1 Background

Lithium-ion batteries (LIBs) have become the dominant energy storage technology across various sectors, including electric vehicles (EVs), portable electronics, and stationary energy storage systems. Their widespread adoption is largely due to their high energy density, long cycle life[3], and relatively low self-discharge rate[5]. As the transition to electrified transportation accelerates, the demand for LIBs with faster charging capability and improved safety continues to grow [6].

One of the key challenges in fast-charging applications is the occurrence of lithium plating, which can lead to rapid capacity degradation[7], increased internal resistance[8], and in extreme cases, thermal runaway[4]. The onset of lithium plating is influenced by several factors, including the charging rate (C-rate)[9], electrode thickness[10], and the intrinsic properties of the electrode materials[12]. While high energy density cathode materials such as NMC811 are widely used in EV batteries[13], they are more prone to side reactions under aggressive cycling[14]. On the other hand, materials like LFP and LFMP offer better thermal stability[15] and longer cycle life[16], but often at the expense of lower specific energy.

Previous studies have explored the role of current density and electrolyte formulation[17] in lithium plating behavior. However, relatively few have systematically examined how cathode material choice and electrode thickness together impact plating under fast-charging protocols[18]. Additionally, much of the existing literature focuses on either simulation or isolated electrochemical results[19], often lacking a controlled comparison across different material systems under consistent testing conditions.

The aim of this thesis is to experimentally investigate the influence of cathode material type (NMC811, LFP, and LFMP), electrode thickness, and charging C-rate on lithium deposition behavior. By combining galvanostatic cycling, electrochemical impedance spectroscopy (EIS), and equivalent circuit modeling, this study aims to identify performance trends and risk factors associated with high rate charging. The results are intended to provide insights for future battery design and help inform optimal charging strategies.

1.2 State of the Art

Recent advances in lithium plating mitigation focus on three main areas: material selection, electrode architecture, and charging protocol design. On the materials side, NMC cathodes dominate EV batteries due to their high energy density (>200mAh/g)[20]. However, they suffer from rapid impedance growth[21] and CEI thickening under high-rate cycling[22]. In contrast, LFP cathodes offer excellent thermal and structural stability with minimal capacity fade under moderate cycling rates[23], although their lower voltage output limits energy density. Emerging LFMP materials bridge this gap by introducing manganese to raise the voltage (4.1V), but Mnš dissolution can trigger SEI degradation and instability during fast charging[24][25].

Electrode thickness plays a critical role in transport kinetics and lithium-ion distribution. While thicker electrodes can deliver higher areal capacity, they also exhibit greater ionic resistance and concentration gradients[26][27], which increase the risk of lithium plating. Prior studies have demonstrated that increasing cathode thickness significantly impacts capacity retention and interfacial stability, especially at elevated C-rates[28][29][30]. However, these effects are rarely examined in systems using lithium metal anodes, where even small perturbations in current distribution can lead to dendritic growth and irreversible lithium loss[31][32].

Several adaptive charging strategies such as voltage-pause intervals and stepped C-rate profiles have shown promise in suppressing plating and stabilizing impedance growth. However, these techniques are typically optimized for graphite or LFP-based systems, and their performance in lithium metal-based cells remains underexplored[33].

To date, limited studies have compared LFMP, LFP, and NMC cathodes under controlled thickness and fast-charging conditions in combination with lithium metal anodes. Moreover, the joint effects of cathode material choice and electrode architecture on impedance growth and plating risk remain insufficiently understood. This thesis aims to address these gaps through a systematic experimental study.

1.3 Battery Terminology

In this section, the terms used in this thesis will be defined. These definitions are in accordance with British and European Standards unless otherwise specified.

1.3.1 End of Life (EoL)

End of Life is a condition reached when the device under test is no longer capable of meeting the applicable goals[34]. It is often defined as the state when the device under test degrades to 80% of its initial capacity.

1.3.2 C-rate

The C-rate is the current normalized with the battery capacity stated by the manufacturer at the reference conditions. That is, a 1,000 mAh battery which is discharged at 1 C-rate (C/1) should ideally deliver the full capacity in one hour. A 10 C-rate (C/0.1) will charge/discharge the battery in 0.1 hour and 0.25 C-rate (C/4) will discharge the battery in 4 hours[35].

1.3.3 Cycle

A sequence of a discharge followed by a charge or a charge followed by a discharge under specified conditions.

1.3.3.1 Open Circuit Voltage ($OCV_{\mathbf{ct}}$)

The Open Circuit Voltage of a cell is the voltage of the cell when it is at electrochemical equilibrium. Depending on the battery size, type and State-of-Charge, the time to reach electrochemical equilibrium varies strongly. For a simple charge-discharge cycle, the close to equilibrium open circuit voltage can be mathematically described by(1.1)

$$OCV_{\text{cte}} = \frac{V_{\text{charge}} + V_{\text{discharge}}}{2} \tag{1.1}$$

Equation 1.1 is applicable when the possible hysteresis eect of the OCV_{cte} is ignored and it is considered temperature independent. cte is the close-to equilibrium condition.

1.4 Research Goals

The primary goal of this research is to explore the impact of varying cathode material thickness and different charging rates on lithium deposition in coin cells, with the aim of developing optimized charging strategies to minimize lithium plating while maintaining battery performance. Specifically, the study focuses on three widely used cathode materials: NMC 811 (Nickel Manganese Cobalt), LFP (Lithium Iron Phosphate), and LMFP (Lithium Manganese Iron Phosphate), combined with lithium metal-based anodes.

1.5 Scope and Limitations

This research focuses on understanding how different electrode materials and thickness and charging rates affect lithium plating in coin cells. The study specifically looks at three types of cathode materials NMC 811 (Nickel Manganese Cobalt),

LFP (Lithium Iron Phosphate), and LMFP (Lithium Manganese Iron Phosphate) paired with lithium metal-based anodes. The research also examines charging rates of 0.1C,1C, 2C, which represent low, medium, and high charging speeds. These rates were chosen to reflect real-world charging scenarios, from everyday use to fast-charging conditions.A key part of the study is the formation process, which is the first charging cycle a battery goes through. During this process, a protective layer called the solid electrolyte interphase (SEI) forms, and this plays a big role in how lithium plating happens.All the batteries used in this study were manually assembled as new cells, ensuring consistency and control over the experimental setup. By focusing on these factors, the research aims to provide a clear picture of how different materials and charging speeds influence lithium plating in a controlled lab setting.

That said, there are some limitations to this study. First, the experiments are done using coin cells, which are small and simple compared to the larger batteries used in real-world applications like electric vehicles. While coin cells are great for controlled experiments, the results might not fully apply to bigger battery systems. Second, the study only looks at specific cathode materials (NMC 811, LFP, and LMFP) and lithium metal-based anodes. There are many other materials used in batteries, so the findings might not apply to all types of batteries. Third, the charging rates tested (0.1C,1C, 2C) dont cover extremely fast charging, which could be important for some applications. Additionally, the experiments are done in a lab under controlled conditions, but in the real world, things like temperature changes, physical stress, and aging can also affect battery performance. And finally ,this work compares lithium plating behavior across three electrode materials using EIS measurements. However, it does not investigate how lithium plating forms or how it evolves over longer-term cycling. As a result, while the study offers useful comparisons, further research is needed to understand the mechanisms and long-term behavior of lithium plating in practical battery applications.

2

Theory

This section introduces the theoretical background relevant to lithium plating detection in lithium-ion batteries. It begins with an overview of the electrode materials used in this study, including NMC, LFP, and LFMP cathodes, as well as a lithium metal-based anode, highlighting their electrochemical properties and relevance to lithium plating behavior. It then explains the mechanism of lithium plating, detailing how it forms during charging and its impact on battery performance and safety. Lastly,the section discusses how charging rate (C-rate) and the cell formation process influence the likelihood of lithium plating, setting the foundation for detecting it through changes in impedance characteristics.

2.1 Electrode Materials

For an energy storage material, the amount of charge that can be stored in a material per unit of mass is crucial. This property is usually called specific capacity. Also, a high potential ensures the requirement of fewer cells for a battery of given voltage. Lithium is an attractive material for batteries with the lowest potential (-3.05 V) vs.hydrogen and the highest specific capacity (3.86 Ah/g)[37]. Apart from many applications in laptops (2.5 billion cells/year), iPods, eReaders and smartphones which are all powered by lithium batteries, the third element in the periodic table (Lithium) may also hold the key to an environmentally sustainable future[36].

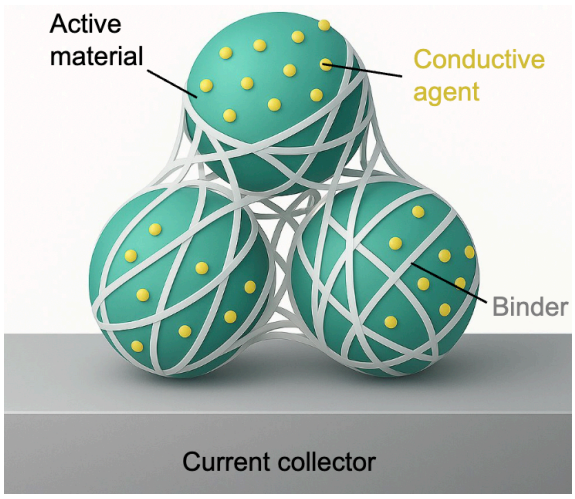

Figure 2.1: Schematic representation of a lithium-ion battery electrode structure

Electrode = Active materials + Nonactive materials (conductive agent/binder)

Provide energy **Support electrode**

The structure of a lithium-ion battery electrode is composed of both active and nonactive materials, each playing a distinct role in ensuring optimal performance. The active material is responsible for storing and delivering energy during charge and discharge cycles. However, to function effectively, it relies on nonactive materials such as conductive agents and binders. The electrochemical processes have been described in the literature [36], and are illustrated schematically in Fig.2.1. The conductive agent forms a network around the active material particles, enhancing electrical conductivity by promoting uniform current distribution and bridging gaps that could otherwise impede electron flow. The binder, typically a polymer, secures the active materials together and attaches them to the current collector, providing mechanical stability and contributing to long-term cycling performance. While nonactive materials do not directly store energy, they are essential for maintaining electrode integrity, supporting efficient charge transfer, and enabling reliable operation, particularly under demanding conditions such as fast charging.

Table 2.1: Cathode materials for Li-ion batteries.

Cathode Material	**Specific Capacity [mAh/g]**	**Notes/Comments**
$LiCoO_2$	140	Good lifetime, high safety risk
$LiFePO_4$	170	Cheap and safe
$LiMn_2O_4$	125	Cheaper, safety better than for Co and Ni
$LiNiO_2$	200	High safety risk, good performance
NMC	203	Popular material from automotive perspective
$LiFeMnPO_4$	150	Popular material

The main cathode materials are summarized in Table 2.1.Cathode materials significantly influence the energy density, rate capability, and cycling stability of lithium-ion batteries. This study investigates three representative cathode chemistries NMC811, LFP, and LFMP chosen for their practical relevance and distinct electrochemical characteristics.This three common cathode materials are summarized in Table 2.2.

NMC811 is widely used in electric vehicles due to its high specific capacity (>200 mAh/g) and a voltage plateau around 3.8 to 4.2 V, yielding excellent energy density. However, it suffers from structural and interfacial instability under aggressive cycling. Key degradation mechanisms include transition metal dissolution (particularly Ni and Mn), cathode electrolyte interphase (CEI) thickening, and lithium plating during fast chargingall of which accelerate impedance growth and capacity loss.

LFP, with its stable olivine structure and an operating voltage of 3.2 to 3.4 V, prioritizes safety, thermal stability, and long cycle life. These attributes make it ideal for safety-critical applications such as grid storage and low-cost EVs. Nevertheless, its lower energy density (150 to 160 mAh/g) stems from a narrower voltage window

and lower specific capacity. Under high C-rates, LFP is also susceptible to lithium plating due to increased polarization.

LFMP is a manganese-doped derivative of LFP, engineered to raise the working voltage to 4.1 V and boost energy density (≈170 mAh/g). While it preserves much of LFP's thermal and structural stability, the introduction of Mn leads to new challenges such as Mnš dissolution under high-rate cycling. This can degrade the solid electrolyte interphase (SEI) and elevate interfacial resistance, compromising long-term performance.

On the anode side, lithium metal is used for its extremely high theoretical capacity (≈3860 to 4250 mAh/g). Despite its promise, it suffers from significant volume changes during cycling, which can induce mechanical stress, dendrite formation, and eventual failure.

By examining these cathodeanode combinations, this study aims to uncover the distinct degradation mechanisms that drive lithium plating under fast-charging conditions. The comparison highlights how cathode chemistry impacts interfacial stability, SEI integrity, and overall cell safety, offering insight into material selection for high-performance, durable lithium-ion batteries.

Table 2.2: Comparison of Three Cathode Materials

Property	**NMC811**	**LFP**	**LFMP**
Nominal Voltage (V)	3.8–4.2	3.2–3.4	∼4.1
Capacity (mAh/g)	>200	∼160	165–175
Energy Density	High	Moderate	Moderate–High
Thermal Stability	Moderate	High	High
Transition Metal Issues	Ni, Mn dissolve	Minimal	Mn dissolve
Typical Applications	EVs, High-end	Buses, Storage	Emerging EVs

2.2 Lithium Plating Mechanism

Significant research interest has been devoted to the development of lithium metal as a negative electrode for rechargeable batteries since the 1970s.1,2 Lithium (Li), with its high theoretical specific capacity (3860 $\mathrm{mAhg^{-1}}$)and lowest electrochemical potential ($-3.04\,\mathrm{V}$ vs. SHE), has since been recognized as an attractive negative electrode material for high energy batteries.However, the industrial deployment of Li metal batteries has been impeded by the critical problems of battery safety and poor cycling lifetime and eciency, all which stem from fundamental issues with the Li plating and stripping process. The intrinsic reactivity of Li metal with electrolyte at low potentials causes their rapid consumption and promotes irreversible solid electrolyte interphase (SEI) formation. Furthermore, mechanical instability of the SEI due to large electrode volumetric changes from repeated Li deposition and stripping

generates nonuniformities at the Li-SEI surface in the form of Li dendrites and filaments, excessively thick SEI layers, or disconnected Li, all of which ultimately give rise to safety hazards and low Coulombic eciency[38]

2.3 Main Factors Affecting Lithium Plating

Extensive research has been conducted to investigate the how, where, and why of lithium plating under both normal and fast charging conditions. Due to its complex nature, the underlying mechanisms remain not fully understood [39].Numerous studies suggest that lithium plating primarily results from three key factors presented in Table 2.3, which include but are not limited to :(i) hazardous operating conditions,(ii) aging of the cell.

Table 2.3: Factors Causing Lithium Plating

Factors	**Causes and Conditions**
Hazardous Operating Conditions	(a) High charging C-rates
Aging of the Cell	(a) Leading to cell unbalance (b) Kinetic degradation (Capacity fade, energy fade, CE decrease, energy efficiency fade and resistance increase)

2.3.1 Hazardous Operating Conditions

Lithium plating typically occurs when batteries operate under harsh conditions such as high charging C-rates .This condition hinders charge transfer kinetics in the electrolyte and slows down solid-state diffusion, causing the anode potential to drop below that of metallic lithium and triggering lithium deposition[40]. Given that such operating extremes are key contributors to lithium plating, this section offers a comprehensive review of the primary parameters that accelerate its formation under this conditions[50].

Fast charging is becoming increasingly important for EVs and other types of applications. Fast charging, which is based on a high charging current (C-rate), has a significant impact on the battery's performance and cyclic life due to accelerated aging. The charging rate is more likely to exceed the intercalation rate during fast charging. At a high C-rate, the amount of Li^+ions moved from the cathode to the anode in the charge-transfer process per unit time increases . Increased charging rates are often associated with higher polarization due to transport and kinetic over potentials, making lithium plating favorable[41]. For example, to recharge a cell in 10 mins, a charge rate of 6 C is required[42]. At this charge rate, Li^+ ions start to accumulate at the anode surface. As the high-rate charging continues, the accumulated Li^+ ions result in a high concentration of Li^+ ions on the graphite surface.

If the concentration at the anode surface is saturated, lithium plating occurs. Furthermore, because fast charging uses a high charge current, more heat is generated. Lithium plating and temperature rise are two well-known issues during the fast charging process.

2.3.2 Aging of the Cell

Even under normal operation conditions, lithium plating can still occur due to the aging of the cell. As mentioned earlier, the most common modes of degradation in the literature are LLI and LAM, where LAM can be further divided into four types based on the affected electrode and the degree of lithiation: loss of active material on the delithiated negative electrode (LAMdeNE), loss of active material on the delithiated positive electrode (LAMdePE), loss of active material on the lithiated negative electrode (LAMliNE), and loss of active material on the lithiated positive electrode (LAMliPE) [31]. After the lithium plating occurs, the side reaction between the plated lithium and the electrolyte generates new SEI, resulting in capacity fading and increased impedance. The changes in these degradation mechanisms can be used to study lithium plating. The analysis of capacity fade curve shapes will provide insight into the mechanism of aging and signs of lithium plating. These curve shapes were classified into three types, linear capacity fade, decelerated capacity fade, and accelerated capacity fade[43][44][45], all of which can be expressed as a function of the number of cycles . In commercial cells, generally, the batteries have a two-stage capacity fade. The capacity fade is fairly constant in the first stage, with a degradation mode related to LLI. Accelerated capacity fade can be found in the second stage of degradation, usually after 500 cycles. The second stage is usually due to LAMdeNE. Ansean et al. showed that LAMdeNE occurs at a pace four times faster than LLI, which causes cell imbalance and over-lithiation of the negative electrode and leads to lithium plating. They found that lithium deposition becomes irreversible at the turning point of sudden capacity loss (curve shape). The second stage usually does not occur due to changes in cell usage, but it may be a product of underlying silent degradation mechanisms from the beginning of life. The type of silent degradation will be affected by the cell chemistry as well as its form factor (pouch and cylindrical cells). These silent degradations have a certain incubation period during which they do not cause any capacity loss. Therefore, it is important to study the modes of degradation, particularly those that may lead to lithium plating. Besides the ratio of LAMNE to the LLI, the plating threshold (LAMNE, PT) is also a predictor of an accelerated degradation stage. Cell design parameters (such as mass ratio), capacity loss, and the two degradation modes (LLI and LAMPE) will affect this value. Values exceeding this threshold cause lithium plating [80]. In another study, Schuster et al. found a significant decrease in capacity at moderate temperatures and charging rates due to lithium plating. They showed that the lithium plating occurred due to significantly decreased ionic kinetics of the graphite as a result of SEI growth and graphite active material loss.

2.4 Suggested Impedance Response Mechanisms

To better understand the electrochemical behavior observed during fast charging, it is essential to examine the impedance response of lithium-ion cells. Electrochemical impedance spectroscopy (EIS) provides insight into various resistance and capacitance elements within the cell, which are often modeled using equivalent circuits.

The most common representation is the Randles circuit, which typically consists of the following components:

- Rs (Solution resistance): Represents ionic resistance in the electrolyte and contact resistances in the electrodes and cell terminals.
- Rct (Charge transfer resistance): Related to the kinetics of the electrochemical reactions at the electrodeelectrolyte interface.
- Cdl (Double layer capacitance): Reflects the capacitive behavior of the electrode surface due to charge separation.
- Zw (Warburg element): Represents diffusion impedance of lithium ions in the solid and liquid phases.

As electrode thickness increases, the diffusion path length also increases, typically leading to a higher Warburg impedance and possible rise in Rct due to non-uniform current distribution. LFMP and NMC811 are particularly sensitive to these effects due to their more complex interphase dynamics.Understanding how each impedance element evolves over cyclingespecially under high C-rateshelps identify lithium plating, SEI degradation, and contact loss.

3
Methods

3.1 Experimental Setup

3.1.1 Electrode and Coin Cell Preparation

The preparation of electrodes started with mixing the cathode slurry using a fixed weight ratio of 7:1:2, representing the active material, conductive carbon black, and PVDF binder. These components were accurately weighed using a Sartorius analytical microbalance with ± 0.1 mg precision. The materials were then mixed thoroughly in a planetary mixer until a uniform slurry was achieved.

The slurry was applied onto carbon-coated aluminum foil using a doctor blade, where the blade gap was adjusted to control the electrode thickness according to the desired loading. After coating, the electrodes were placed in a vacuum oven and dried at 80°C for at least 24 hours to ensure complete solvent removal and proper binder adhesion.

Once dried, circular discs with a radius of 0.6 cm were punched out using a precision cutter to maintain consistent electrode size across all samples. Each disc was weighed to determine the active material loading, which was essential for later analysis of electrochemical performance. The electrodes were labeled and kept in a desiccator before assembly.

The coin cells were assembled in an argon-filled glovebox to avoid moisture and oxygen exposure. Each cell included the prepared cathode, a lithium metal-based anode, a LiPF-based electrolyte, and a porous separator, with lithium metal serving as the counter electrode. After stacking the components, the cells were sealed using a hydraulic crimping tool to ensure durability and prevent leakage.

Following assembly, the cells were tested on a Chalmers-designed test bench, which was programmed to run predefined charging protocols (0.1C, 1C, and 2C). Throughout the tests, voltage, current, and impedance data were recorded at 10-second intervals. All measurements were conducted at room temperature (25°C).

An overview of the electrode preparation and coin cell assembly process is shown in Fig.3.1 and Fig.3.2, summarizing the steps from initial weighing to final cell crimping. These procedures were carefully controlled to ensure uniformity across all test samples. For each cathode material and each electrode thickness, at least three coin

cells were prepared. This was done both to prevent the risk of failure during testing and to ensure that the dataset was sufficient for meaningful comparison and analysis.

By standardizing electrode loading, size, and assembly conditions inside a glovebox, the risk of variation was minimized. The cells prepared using this workflow were then used in the electrochemical tests described in the next section.

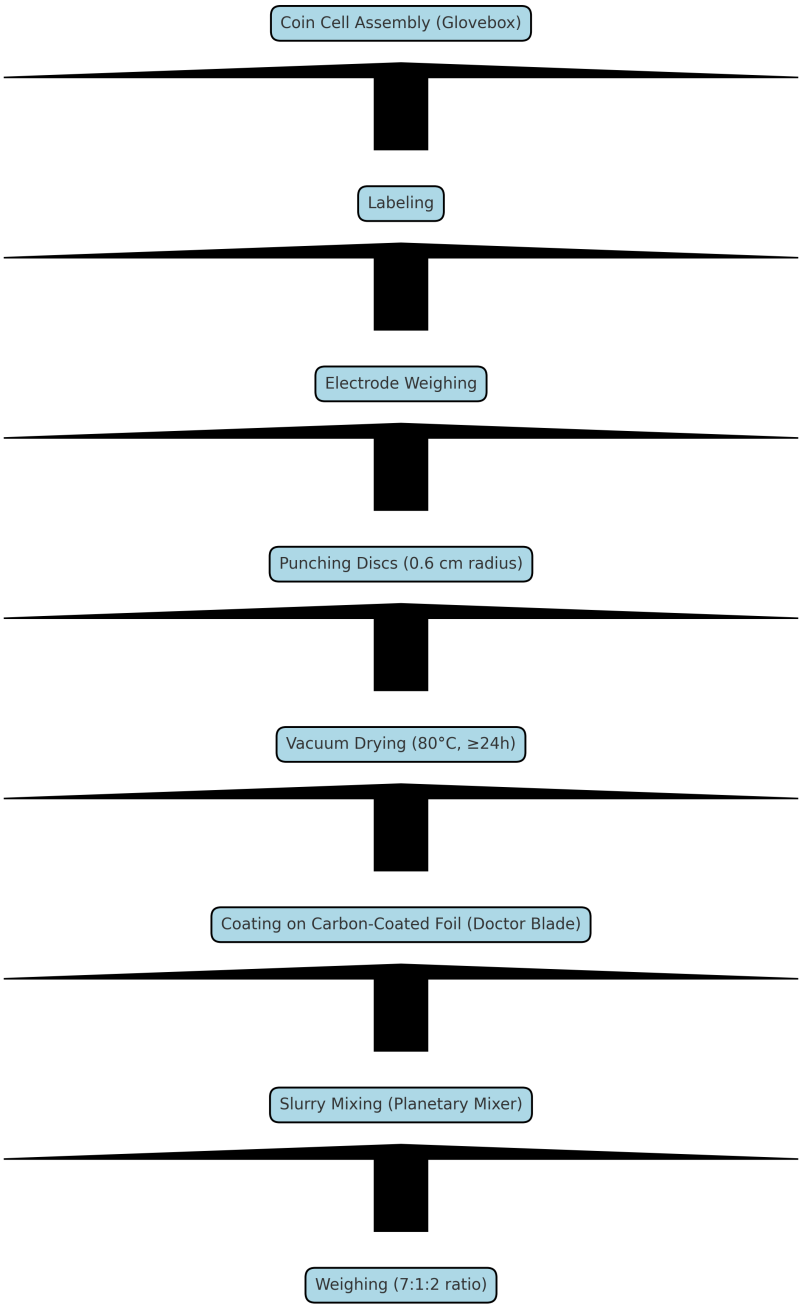

Figure 3.1: Electrode Preparation Coin Cell Assembly Flowchart

(a) Slurry

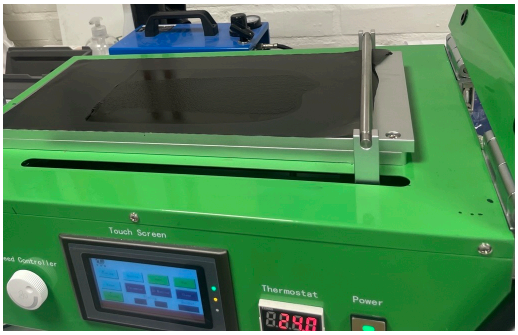

(b) Coating the electrode

(c) Wet electrode

(d) Dry electrode

Figure 3.2: The fabrication process of battery electrodes, illustrating key steps from slurry preparation (a), electrode coating (b), wet electrode formation (c), to the final dry electrode (d).

3.2 Measurement Techniques

All measurements in this study were carried out using the coin cells described in Section 3.1.1. After assembly, each cell was tested on a Chalmers-designed test bench under controlled lab conditions. The bench was programmed to follow a sequence of charging protocols with increasing current rates (0.1C, 1C, and 2C), allowing the evaluation of how different materials and electrode configurations respond under stress.

Voltage, current, and impedance data were logged every 10 seconds to capture changes throughout each cycle. The goal was to track how the cells behave as the charging rate increases, especially with regard to lithium plating and capacity fade. All tests were performed at room temperature (25°C), and the same conditions were used across all samples to ensure comparability.

3.2.1 Cycling Protocol

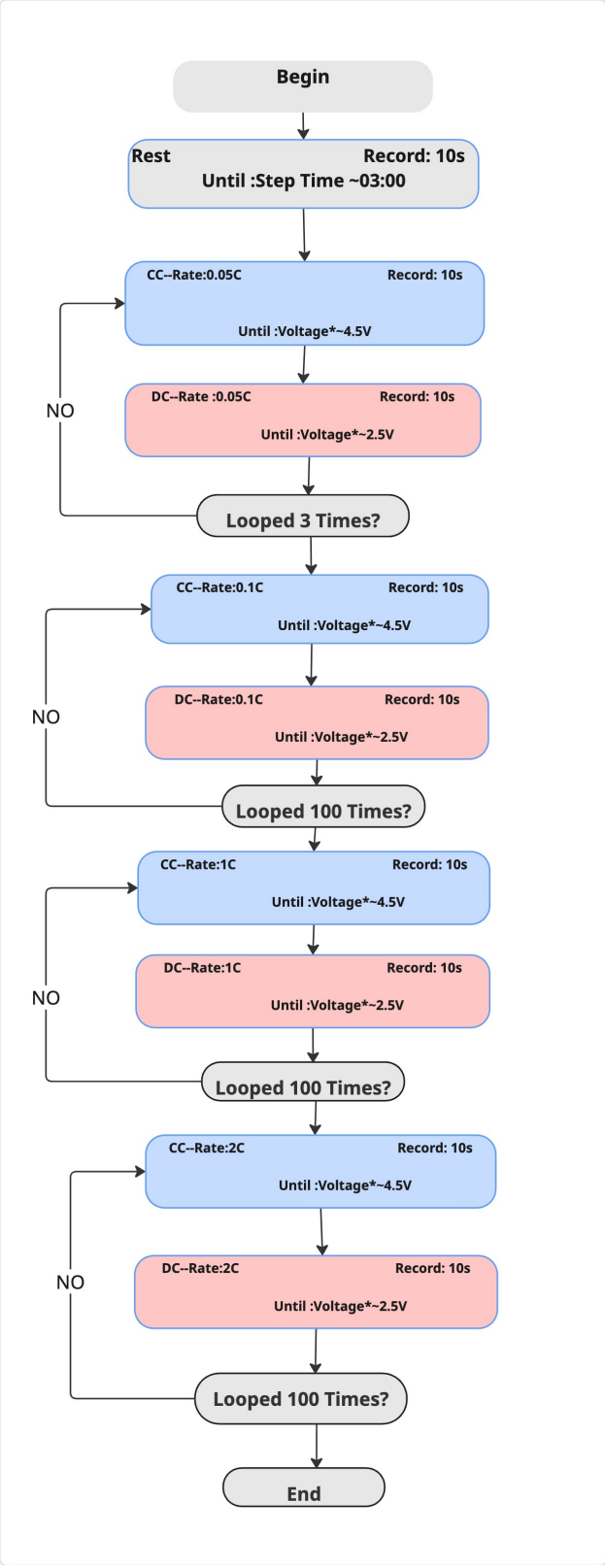

Figure 3.3: Test protocol for cycling from slow to fast charging

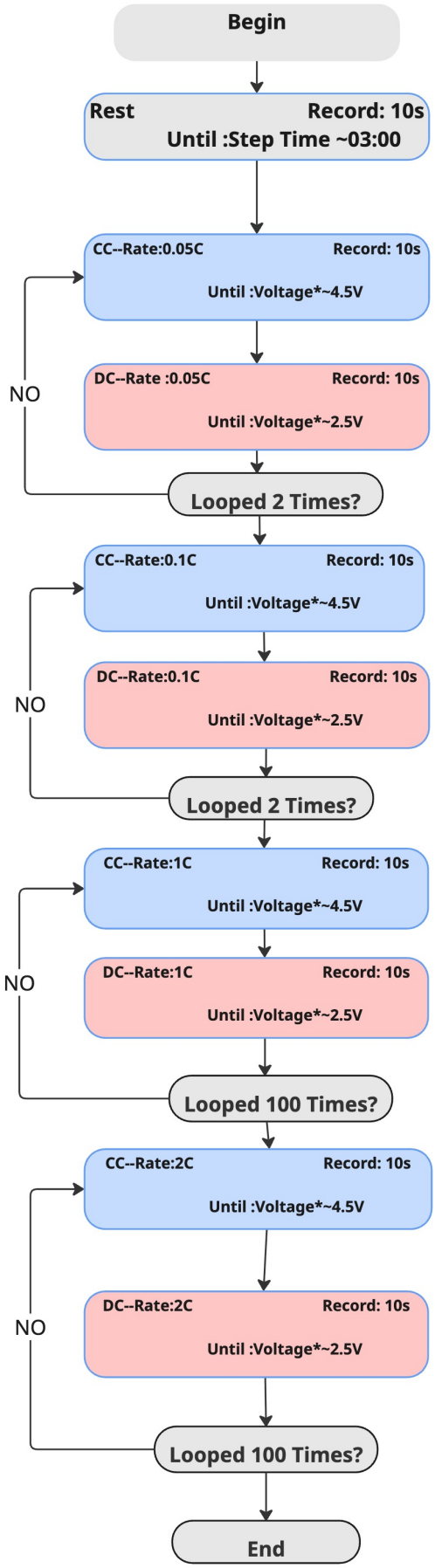

Figure 3.4: Test protocol for fast charging cycling immediately after activation

Step 1: Activation Phase

All cells underwent an initial activation process to stabilize the Solid Electrolyte Interphase (SEI), which is critical for long-term cell performance and safety. The activation began with a low current charge at 0.05C, allowing for gentle formation of the SEI layer, minimizing the risk of lithium plating and ensuring uniform layer growth on the anode surface.

Following this, each cell was subjected to three controlled formation cycles at a slightly higher rate of 0.1C, within a defined voltage window:2.5 to 4.5 V for cells utilizing NMC-based cathodes.2.0 to 3.6 V for cells with LFP/LMFP cathodes.This careful conditioning phase is essential to promote stable electrochemical behavior by optimizing SEI formation, which acts as a protective barrier, reducing electrolyte decomposition and preventing capacity loss during subsequent cycling. The slow charging and discharging rates were chosen to avoid mechanical stress and thermal effects, both of which can negatively impact SEI integrity.

The detailed protocol for this activation phase is illustrated in Figure 3.3 for the comparative group, where this activation is followed directly by high-rate cycling.

Step 2: Baseline Cycling

For the control group, following activation, the cells underwent an additional 100 cycles at 0.1C to establish a stable baseline for capacity retention, Coulombic efficiency, and SEI stability. This phase was essential to replicate typical low-stress usage conditions prior to subjecting the cells to more aggressive cycling.

This step served two main purposes: To promote further maturation of the SEI layer under gentle cycling conditions, enhancing its mechanical strength and ionic conductivity.To generate reference data for long-term performance, facilitating direct comparison with cells exposed to immediate high-rate cycling.

By maintaining a consistent 0.1C rate and strictly controlling voltage and temperature parameters, this baseline phase offered valuable insights into the natural aging behavior of the cells, free from high-rate stress influences.

The complete protocol for this group, encompassing both the baseline phase and subsequent high-rate cycling, is illustrated in Figure 3.4 .

Step 3: High-Rate Cycling

After baseline cycling, the cells were subjected to high-rate charge and discharge cycles at 1C and 2C rates, with 100 cycles performed at each rate. The voltage limits were maintained strictly within the predefined window, and all tests were conducted at a controlled temperature of 25°C to ensure consistency. This phase was designed to evaluate the cell's performance, capacity retention, and SEI stability

under more demanding conditions that simulate real-world fast-charging scenarios. For a detailed overview of the cycling protocol applied during this step, see Figure 3.3, which illustrates the sequence and conditions of the fast-charging cycles.

Step 4: Comparative Group

To assess the influence of SEI formation during low-rate cycling on subsequent high-rate performance, a comparative group of cells was tested. These cells bypassed the baseline cycling phase and proceeded directly to high-rate cycling at 1C and 2C after the initial activation process. This approach aimed to highlight differences in degradation behavior and performance without the stabilizing effect of extended low-rate cycling. Following the high-rate cycles, Electrochemical Impedance Spectroscopy (EIS) measurements were conducted to analyze changes in internal resistance and SEI characteristics. The detailed test protocol for this comparative group is illustrated in Figure 3.4, showing the direct transition from activation to fast-charging cycles without preliminary low-rate cycling.

3.2.2 Electrochemical Impedance Spectroscopy (EIS) Analysis

Electrochemical Impedance Spectroscopy (EIS) was employed to investigate the internal resistance and interfacial characteristics of the cells after the completion of the full cycling protocols (see Figures 1 and 2). All measurements were conducted at open-circuit voltage (OCV) using a frequency range of 100 kHz to 10 mHz and a 10 mV AC amplitude, providing a non-destructive method to assess impedance-related changes due to cycling.

In this study, EIS measurements were performed only once, and only after all cycling phases were completed. This approach was adopted in consideration of the limited capacity testing resources available in the laboratory, and because the aim of this thesis is not to monitor the detailed evolution of impedance throughout cycling, but rather to confirm the presence and scale of impedance development after full electrochemical stress.

To ensure a valid comparison across materials, one representative cell per electrode material was selected for EIS testing. All tested cells used electrodes of the same thickness, deliberately controlled to eliminate the influence of geometrical factors. This is important because the specific resistance is known to increase with increasing electrode thickness [48], and controlling this variable allows observed differences to be attributed primarily to the cycling history.

Two experimental groups were included:

Table 3.1: EIS Measurement Timing and Purpose

Test Group	**EIS Measurement Timing**	**Purpose of EIS Analysis**
Control Group	After all cycling phases were completed	To assess cumulative impedance evolution after prolonged low- and high-rate cycling, focusing on SEI stability and charge transfer resistance.
Comparative Group	After all cycling phases were completed	To evaluate impedance behavior without baseline cycling, highlighting the impact of immediate high-rate stress on SEI and interfacial resistance.

A control group, which followed the full protocol including activation, baseline low-rate cycling (0.1C), and subsequent high-rate cycling (1C and 2C).

A comparative group, which underwent activation followed immediately by high-rate cycling, omitting the baseline phase.

Voltage and current profiles were logged at 1-second intervals throughout the cycling period, providing high-resolution data on capacity retention and Coulombic efficiency, and serving as context for interpreting impedance results.

All impedance spectra were acquired using the Biologic VMP-3 workstation, and fitted using semi-empirical equivalent circuit models in EC-Lab software. These models were based on modified Randles-type circuits tailored to each material, incorporating:

Ohmic resistance (R_s): reflecting bulk electrolyte and contact resistance

CEI resistance (R_{CEI}): capturing resistive behavior of the solid electrolyte interphase

Charge transfer resistance (R_{ct}): associated with electrochemical kinetics at the electrode/electrolyte interface

Constant phase elements (CPEs): modeling non-ideal capacitive behavior due to surface inhomogeneities

Warburg elements: representing solid-state diffusion limitations.

The focus of the analysis was to determine the cumulative impact of cycling on impedance characteristics, rather than to quantify exact changes over time, which would require a broader dataset and more granular testing.

4

Result and Discussion

4.1 Capacity and Efficiency Analysis

4.1.1 Influence of Electrode Thickness

For each cathode material (NMC, LFP, LFMP), three electrode thicknesses (~2 mg, 4 mg, and 7 mg) were analyzed to assess how thickness influences performance.

Figures 4.1 to 4.3 illustrate the specific capacity and Coulombic efficiency (CE%) as a function of cycle number under low-to-high rate cycling conditions (0.1C 1C 2C).

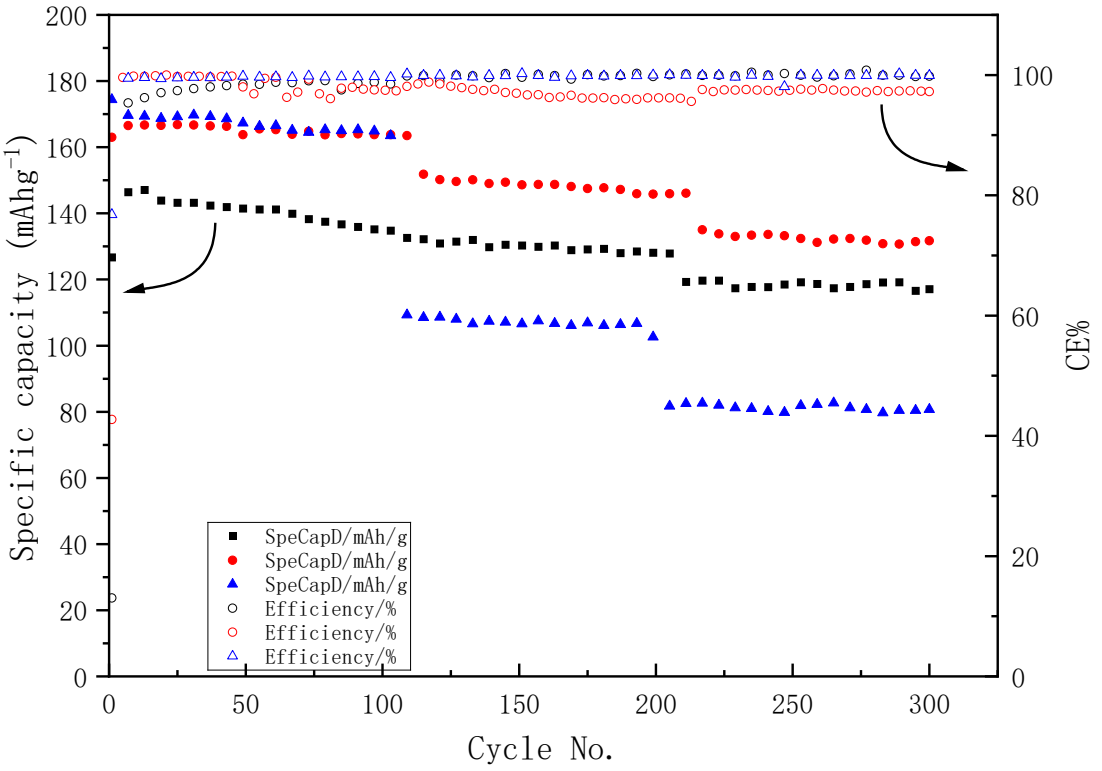

Figure 4.1: Comparison of LFP with Three Different Thicknesses

This figure illustrates the specific capacity and Coulombic efficiency (CE) of Lithium Iron Phosphate (LFP) cathodes across three electrode thicknesses (2 mg, 4 mg, and 7 mg) under varying charging rates (0.1C to 2C). Thin electrodes (2 mg) exhibit the

highest capacity retention and stable CE (>99%), indicating minimal polarization and efficient lithium-ion transport. Moderate thickness (4 mg) shows slight capacity fade at 2C, while thick electrodes (7 mg) suffer from significant capacity degradation and CE fluctuations, likely due to increased ionic resistance and non-uniform lithium deposition under high-rate conditions. The results highlight LFPs inherent stability but emphasize that excessive thickness exacerbates kinetic limitations, even for this robust material.

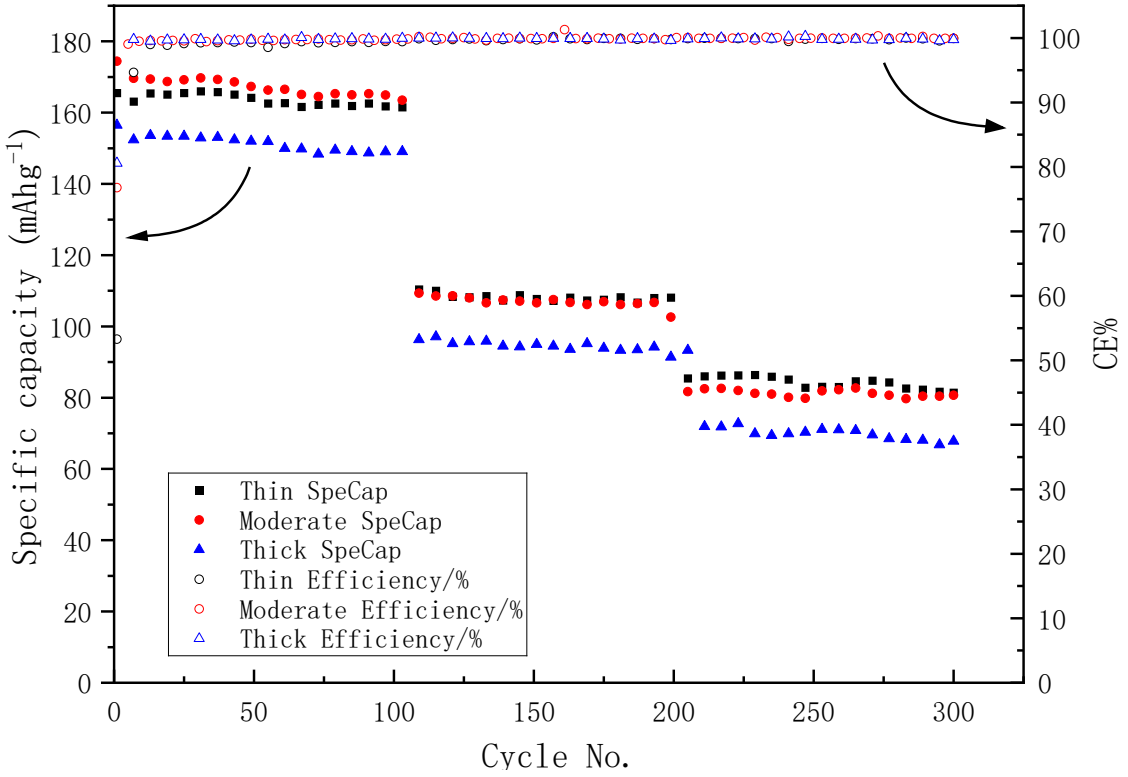

Figure 4.2: Comparison of LFMP with Three Different Thicknesses

This figure 4.2 evaluates Lithium Manganese Iron Phosphate (LFMP) cathodes with three thicknesses. Thin electrodes (2 mg) maintain stable cycling performance with 80% capacity retention, whereas thicker electrodes (7 mg) display rapid capacity fade and erratic CE, particularly at 2C. The sharp decline in thick LFMP electrodes suggests aggravated manganese dissolution and interfacial instability under high-rate charging, exacerbated by prolonged diffusion paths. LFMPs sensitivity to electrode thickness underscores the need for optimized mass loading to balance energy density and electrochemical stability in fast-charging applications.

A. Capacity Retention

Capacity was normalized to the initial value and plotted versus cycle number. As shown in Figures 4.4 to 4.6, thinner electrodes demonstrated better rate performance and capacity retention during 2C cycling, while thicker electrodes experienced faster capacity fade due to increased ionic transport limitations.

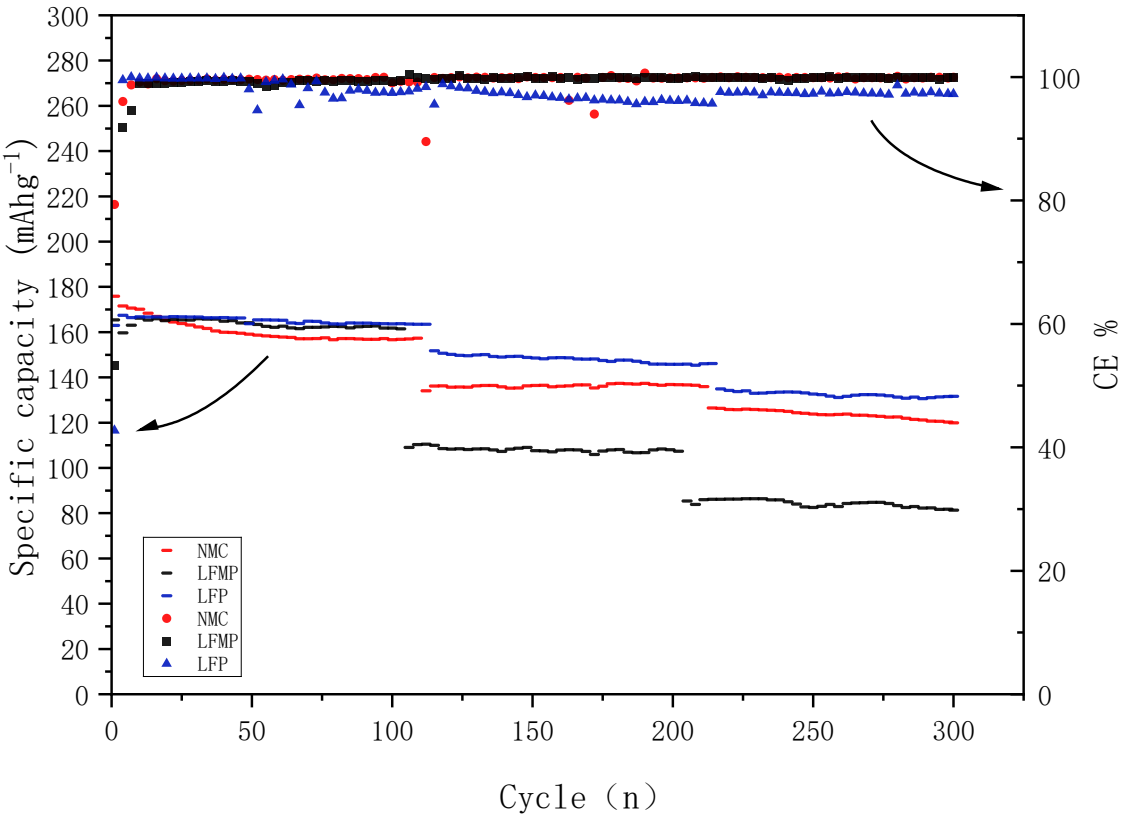

Figure 4.3: Specific Capacity and CE of NMC811, LFP, and LFMP with thin electrodes

This figure compares thin electrodes (2 mg) of NMC811, LFP, and LFMP. NMC811 delivers the highest initial capacity (>160 mAh/g) but exhibits gradual capacity fade and rising impedance at 2C, linked to nickel-induced structural degradation. LFP demonstrates the most stable performance with minimal capacity loss and consistent CE, reflecting its robust olivine structure. LFMP shows intermediate capacity but higher CE variability, indicating partial susceptibility to interfacial side reactions. The contrast highlights the trade-offs between energy density (NMC811) and stability (LFP) in thin electrodes.

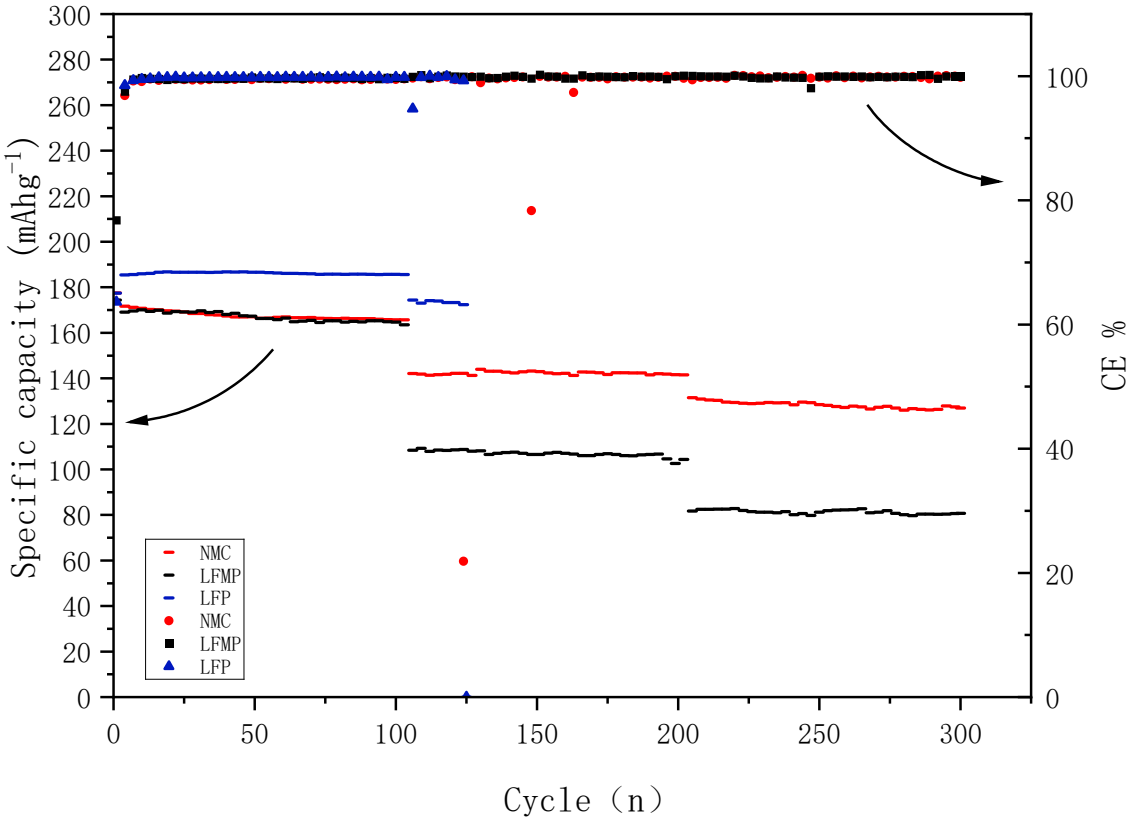

Figure 4.4: Specific Capacity and CE of NMC811, LFP, and LFMP with moderate electrodes

For moderate thickness (4 mg), NMC811 retains high capacity but accelerates degradation at 2C, with CE dropping below 98%. LFP maintains stable capacity and CE (>99%), confirming its resilience to moderate thickness. LFMP exhibits a steeper capacity fade compared to thin electrodes, suggesting that even moderate thickness amplifies its sensitivity to high-rate cycling. The data reinforce that LFPs structural stability mitigates thickness-related challenges, while NMC811 and LFMP require stricter thickness control for high-rate applications.

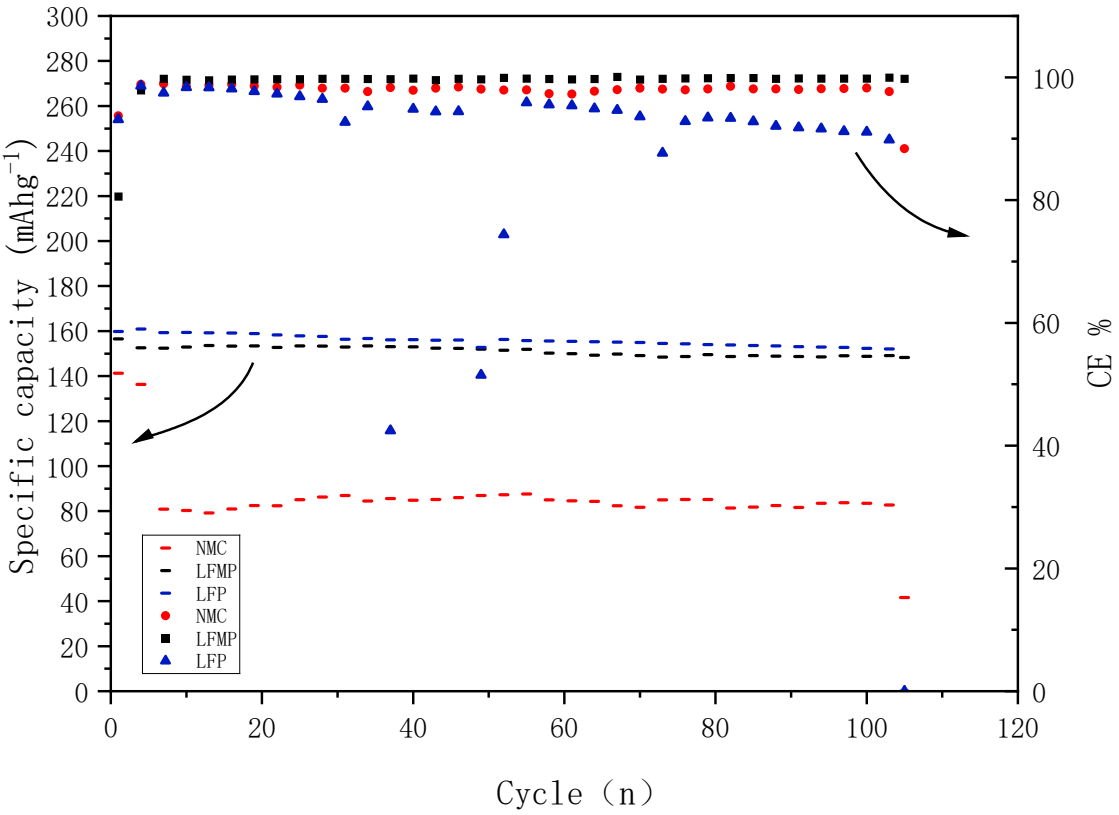

Figure 4.5: Specific Capacity and CE of NMC811, LFP, and LFMP with thick electrodes

Thick electrodes (7 mg) reveal stark performance differences. NMC811 suffers severe capacity loss (>30% after 100 cycles) and CE instability, driven by CEI growth and lithium plating. LFPs capacity remains stable, though CE fluctuations emerge at 2C, indicating mild polarization. LFMPs thick electrodes collapse rapidly, with CE dipping below 95%, likely due to Mn dissolution and SEI degradation. The results underscore that thick electrodes amplify material-specific weaknesses, making LFP the most viable for high-loading designs, while NMC811 and LFMP demand advanced engineering to offset thickness-induced limitations.

B. Coulombic Efficiency (CE)

CE remained above 99% for all materials at low to moderate thicknesses. However, thick electrodes showed larger fluctuations, especially for LFMP, suggesting greater side reactions or possible lithium plating.

C. Degradation Trends

Capacity degradation rate was steeper for thicker electrodes, correlating with increased internal resistance and non-uniform current distribution.

4.1.2 Comparison Across Materials (Fixed Thickness)

At a fixed electrode mass of approximately 4mg, the three cathode materials demonstrated distinct performance profiles. NMC811 exhibited the highest initial capacity but suffered from faster degradation under 2C cycling, likely due to nickel-induced structural instability. LFP maintained the most stable cycling behavior, with minimal capacity fade and consistently high Coulombic efficiency. LFMP delivered moderate performance but showed greater sensitivity to abrupt high-rate charging when not preconditioned.

In terms of impedance evolution, NMC811 experienced the most significant rise in charge transfer resistance (R_{ct}, up to 45%), while LFP showed only slight increases in both SEI resistance and R_{ct}, reflecting its stable interfacial characteristics. LFMP presented moderate impedance growth, which is likely linked to manganese dissolution and interfacial instability. Table 4.1 summarizes the key performance metrics.

4.2 Electrochemical Impedance Spectroscopy (EIS) and Model Fitting

Electrochemical impedance spectroscopy (EIS) was performed after completing 100 low-rate cycles, followed by a period of high-rate cycling.

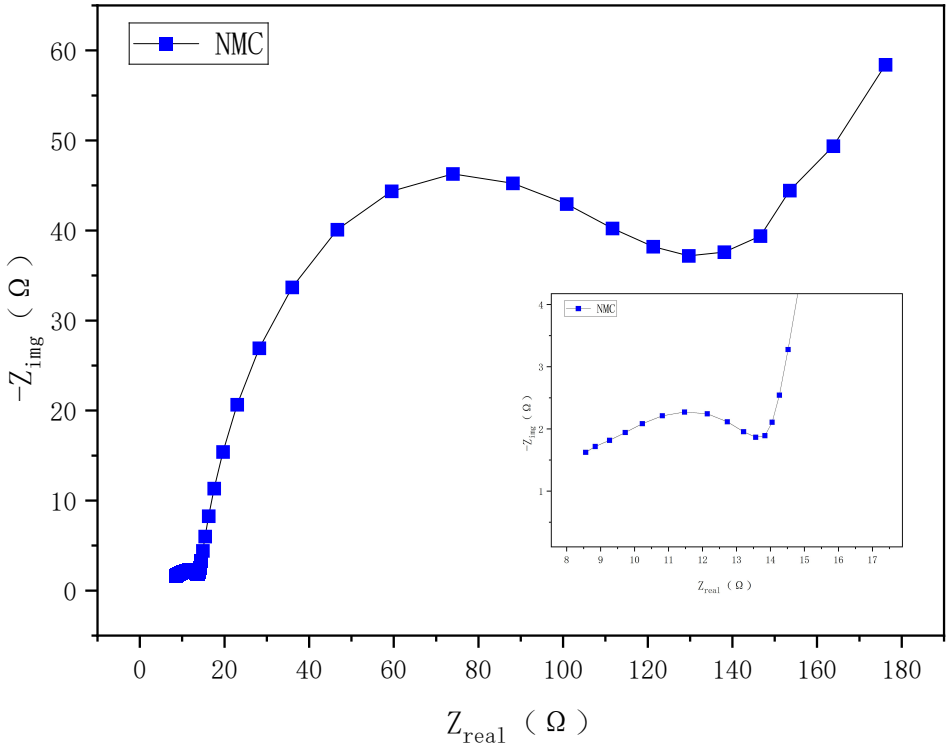

Figure 4.6: Impedance changes over time for the NMC811-based electrode

This figure depicts the impedance evolution of NMC811 cathodes across cycling phases. The dominant increase in impedance stems from the cathode-electrolyte

interphase (CEI) resistance, which rises to approximately 125 Ω after prolonged high-rate cycling. The charge transfer resistance (R_{ct}) also grows moderately, indicating sluggish reaction kinetics due to nickel/manganese dissolution and CEI thickening. The cumulative impedance growth correlates with NMC811s observed capacity fade, highlighting its vulnerability to interfacial degradation under aggressive charging. These results underscore the trade-off between NMC811s high energy density and its long-term stability in fast-charging applications.

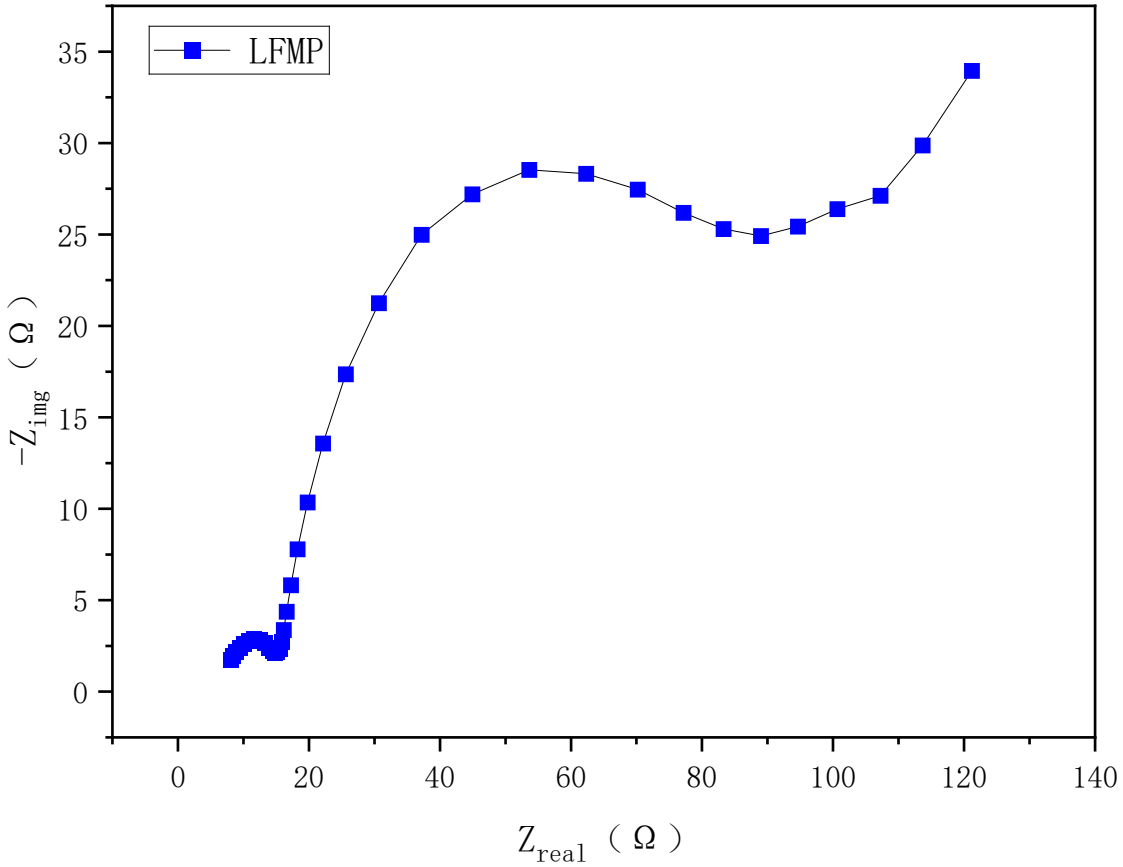

Figure 4.7: Impedance changes over time for the LFMP-based electrode

LFMP electrodes exhibit a distinct impedance profile, with charge transfer resistance(R_{ct})surging to ≈ 180 Ω, significantly higher than CEI or ohmic contributions. This reflects sluggish electrochemical kinetics, likely exacerbated by manganese dissolution and unstable SEI formation under high-rate cycling. Unlike NMC811, LFMPs CEI resistance remains relatively low (6 Ω), suggesting its degradation is primarily interfacial rather than structural. The pronounced Rct rise aligns with LFMPs rapid capacity fade, emphasizing its sensitivity to kinetic limitations in fast-charging scenarios.

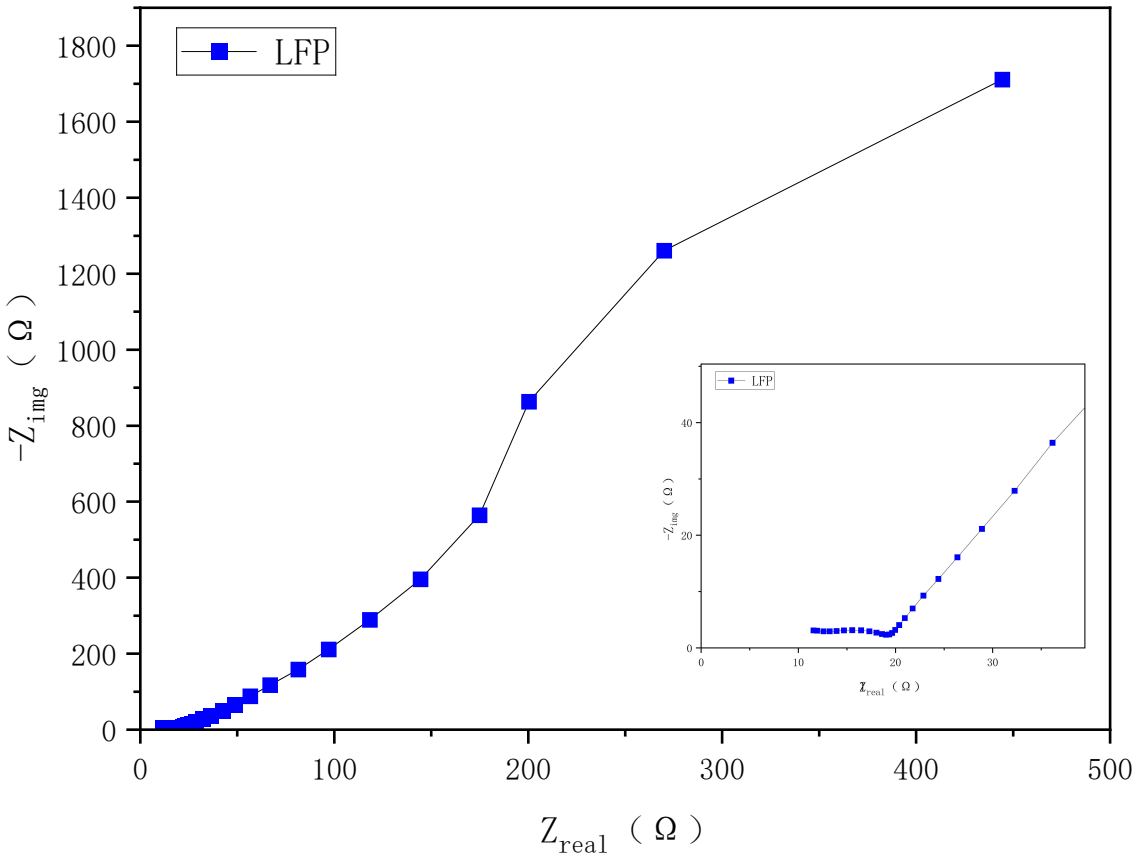

Figure 4.8: Impedance changes over time for the LFP-based electrode

LFP electrodes demonstrate minimal impedance growth across all components (R_s,R_{CEI}, and R_{ct}), maintaining stable values even after 2C cycling. The ohmic resistance (R_{s}) and CEI resistance (R_{CEI}) remain below 10 Ω, while R_{ct} stays under 8 Ω, reflecting robust interfacial stability and efficient charge transfer. This aligns with LFPs superior capacity retention and consistent Coulombic efficiency, reinforcing its suitability for applications prioritizing longevity over ultra-high energy density.

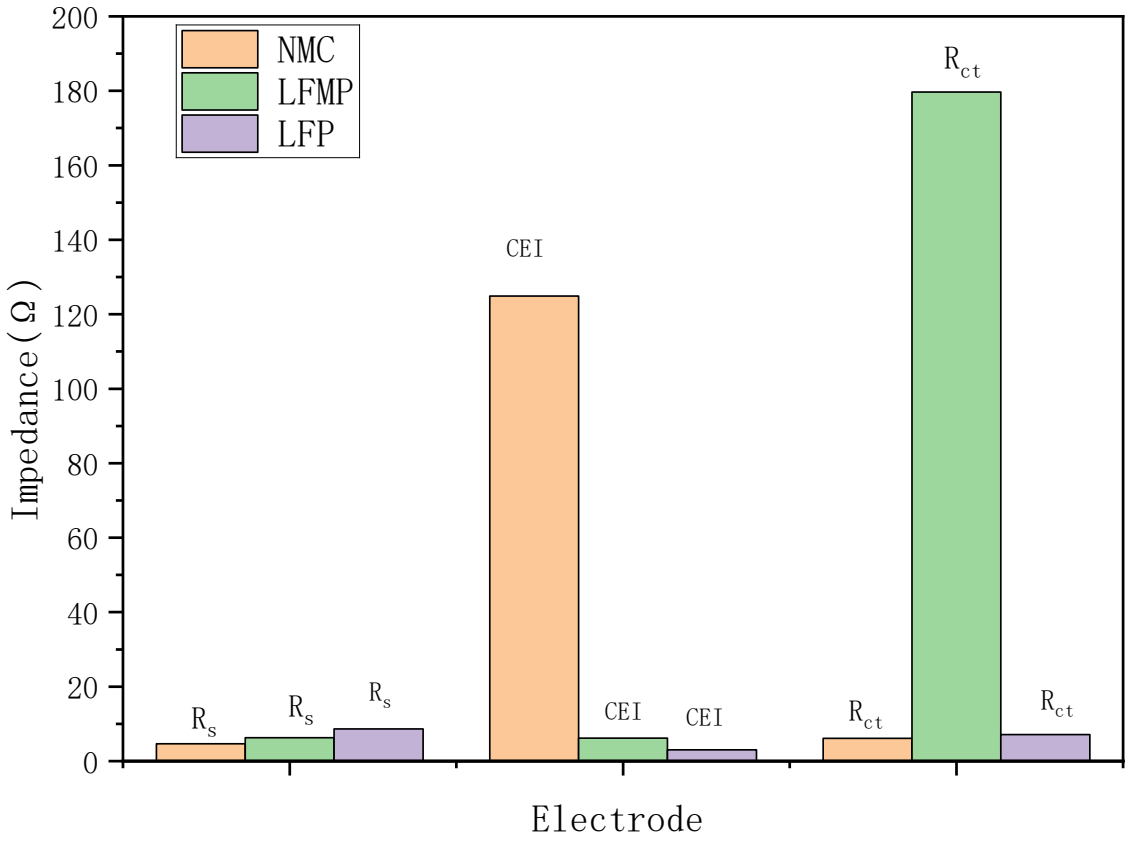

Figure 4.9: Impedance summary

This summary compares impedance characteristics of NMC811, LFMP, and LFP after cycling. NMC811 shows dominant CEI resistance (124.9 Ω), LFMP exhibits extreme R_{ct} (179.7 Ω), and LFP maintains balanced, low resistance across all parameters. The stark contrasts highlight material-specific degradation mechanisms: NMC811s interfacial instability, LFMPs kinetic limitations, and LFPs structural resilience. These findings emphasize that cathode chemistry dictates impedance behavior, guiding material selection for applications balancing energy density, rate capability, and cycle life.

To better quantify the impedance behavior, all EIS spectra were fitted using equivalent circuit models in BT-lab software. The models included Rs, R_{CEI}, R_{ct}, and Warburg diffusion components.Due to the minimal impact of electrode thickness on R_{ct} for the same materialcite[49], electrodes with the same thickness were selected across the three cathode types for EIS measurements.

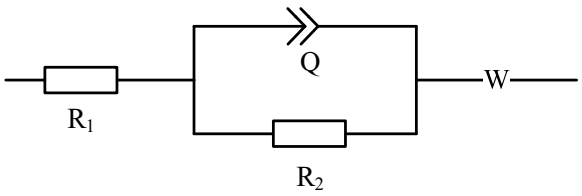

Figure 4.10: Equivalent circuit of EIS-based model for LFP electrode material

This figure 4.10 presents a semi-physical impedance model tailored for Lithium Iron Phosphate (LFP) cathodes, combining theoretical principles and empirical fitting. The model includes key components such as ohmic resistance (R_s), representing bulk electrolyte and contact resistance; CEI resistance (R_{CEI}), capturing the stable solid-electrolyte interphase; and charge transfer resistance (R_{ct}), associated with the efficient lithium-ion insertion/extraction kinetics. A constant phase element (CPE) accounts for non-ideal capacitive behavior due to surface inhomogeneities, while a Warburg element (W) models solid-state diffusion limitations. The minimal growth of R_{CEI} and R_{ct} in LFP aligns with its stable cycling performance, reflecting robust CEI integrity and low polarization even under high-rate charging. This model underscores LFPs structural resilience and validates its suitability for applications requiring long-term stability.

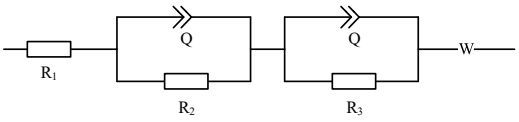

Figure 4.11: Equivalent circuit of EIS-based model for LFMP and NMC electrode material

This figure 4.11 shows impedance models for LFMP and NMC811 cathodes, highlighting material-specific degradation mechanisms. For LFMP, the model features a significantly elevated charge transfer resistance ($R_{ct} \approx 180\ \Omega$), attributed to manganese dissolution and unstable interfacial kinetics under fast charging. A Warburg

element dominates diffusion impedance, reflecting prolonged ion transport paths. In contrast, NMC811 exhibits prominent CEI resistance ($R_{CEI} \approx 125\ \Omega$), driven by nickel/manganese dissolution and cathode-electrolyte interphase thickening. Both models incorporate CPEs to address surface heterogeneity but differ in resistance distribution: LFMPs degradation centers on sluggish charge transfer, while NMC811s stems from interfacial instability. These models elucidate why LFMP and NMC811 suffer faster capacity fade compared to LFP, emphasizing the need for material-specific optimizations to mitigate high-rate limitations.

4.3 Impedance under three different electrode

Summary Table: Material vs. Thickness Performance

Table 4.1: Material vs. Thickness Performance

Material	**Mass** (mg)	**After 100 cycles at 1C and 2C**		
		$R_{\mathbf{s}}$	$R_{\mathbf{SEI}}$	$R_{\mathbf{ct}}$
	2.121	-	-	-
NMC 811	4.088	-	-	-
	7.31	4.67	124.9	6.117
	2.422	-	-	-
LFP	3.906	-	-	-
	6.853	8.6181	3.05	7.113
	2.52	-	-	-
LFMP	3.906	-	-	-
	6.076	6.272	6.17	179.7

The EIS impedance analysis reveals distinct differences in resistance contributions across the three electrode materials. For NMC, the dominant resistance arises from the CEI (cathodeelectrolyte interphase) layer, reaching approximately $125\,\Omega$, indicating significant interfacial impedance buildup.

In contrast, LFMP shows a much lower CEI resistance but exhibits a remarkably high charge transfer resistance(R_{ct}),around $180\,\Omega$, suggesting slower electrochemical kinetics at the interface. LFP demonstrates relatively balanced and minimal impedance values across all components,R_{s}, CEI, and R_{ct}, highlighting its stable interfacial properties and efficient charge transfer behavior. These differences underscore the influence of material selection on interfacial characteristics and overall electrochemical performance .

4.4 Discussion

The results highlight that both cathode chemistry and electrode thickness play decisive roles in dictating lithium plating behavior under fast-charging conditions.

NMC811, while delivering the highest initial capacity, exhibited accelerated impedance growth and capacity fade during aggressive cycling, consistent with transition-metal dissolution and CEI thickening. LFP, in contrast, maintained remarkable stability across different thicknesses and C-rates, with minimal impedance increase, reflecting the robustness of its olivine structure. LFMP demonstrated intermediate performance: it benefitted from higher voltage compared to LFP but proved highly sensitive to electrode thickness and abrupt fast-charging, which triggered manganese dissolution and elevated charge-transfer resistance. These findings confirm that while energy density is strongly influenced by material selection, interfacial stability ultimately governs long-term fast-charging durability. Electrode thickness further amplified these material-specific behaviors: thin electrodes enabled efficient ion transport and stable Coulombic efficiency, whereas thick electrodes suffered from increased polarization and non-uniform current distribution, accelerating plating and side reactions. Tailored charging strategies were also found to be critical, with stepwise charging protocols mitigating stress and stabilizing LFMP in particular, underscoring the importance of coupling material design with operational control.

At the same time, the study reveals limitations that point to promising directions for future work. The tests were conducted on coin cells and within a limited number of cycles, meaning that long-term degradation pathways and practical cell-scale behavior remain to be validated. Moreover, the impedance analysis was performed only at the end of cycling, capturing cumulative effects but not the dynamic evolution of interfacial processes. To address these gaps, future research should incorporate extended cycling campaigns, in-situ/operando diagnostics, and interface engineering approaches such as protective coatings or advanced electrolytes. Exploring electrode architectures with graded porosity or 3D designs may help overcome the transport limitations observed in thick electrodes, while adaptive charging protocols informed by real-time impedance feedback could enable safe fast charging across chemistries. By extending the scope in these directions, the present findings can be translated into practical solutions for next-generation lithium-ion batteries.

5

Conclusion and Future work

This thesis has explored how cathode chemistry, electrode thickness, and charging protocol collectively influence lithium plating and degradation behavior in lithium-ion batteries with lithium metal-based anodes. The comparative study of NMC811, LFP, and LFMP demonstrated clear material-dependent trade-offs. NMC811 achieved the highest specific capacity but suffered from rapid impedance rise and interfacial instability during fast charging, consistent with CEI thickening and transition-metal dissolution. LFP, in contrast, provided stable cycling performance across different loadings and charging conditions, confirming its suitability for applications prioritizing longevity and safety over maximum energy density. LFMP offered an intermediate option, with a higher voltage than LFP but heightened sensitivity to both electrode thickness and abrupt high-rate cycling, where manganese dissolution and interfacial degradation accelerated capacity fade. These results highlight that while energy density is governed largely by material chemistry, the long-term stability of fast charging is strongly dependent on interfacial robustness.

Electrode architecture emerged as an equally important factor. Thin electrodes consistently preserved high Coulombic efficiency and restrained impedance growth, whereas thick electrodes amplified transport limitations, concentration polarization, and non-uniform current distribution, which in turn increased the likelihood of plating and accelerated performance decay. This trade-off illustrates the central design dilemma of balancing areal capacity with fast-charging durability. Charging protocol was shown to act as a critical external lever: stepwise fast charging effectively mitigated interfacial stress and stabilized performance, particularly for LFMP, while immediate exposure to high rates worsened degradation. Together, these findings confirm that safe and efficient fast charging requires not only material selection but also deliberate design of electrode structures and operational strategies.

In general, the study provides a systematic experimental framework that links materials, electrode design, and charging conditions to degradation behavior under fast charging. The findings contribute to scientific understanding by clarifying why Ni-rich cathodes trade stability for energy density, why LFP maintains superior robustness despite lower capacity, and why LFMP requires careful activation and tailored charging. At the same time, the results hold practical value, offering guidance for industrial battery development where energy density, cycle life, and charging speed must be balanced. By combining controlled laboratory experiments with impedance-based diagnostics, this thesis advances both academic knowledge and applied design principles for next-generation lithium-ion batteries.

5.1 Future Work

Future studies should extend beyond coin-cell configurations to long-term cycling of pouch or cylindrical cells, including operation under varied temperatures, mechanical stresses, and extreme fast-charging regimes (>6C). Incorporating in-situ and operando diagnostics such as Raman spectroscopy, neutron diffraction, or X-ray tomography would provide real-time insight into lithium plating, SEI/CEI evolution, and interfacial instability. Parallel efforts in interface engineeringsuch as ultrathin coatings, advanced electrolyte formulations, or polymerceramic hybrid electrolytescould mitigate the limitations observed in Ni-rich and Mn-containing chemistries. On the design side, electrode architectures with graded porosity or 3D conductive frameworks should be explored to reduce transport bottlenecks in thick electrodes, enabling high areal capacity without compromising durability. Finally, adaptive charging protocols guided by machine-learning models trained on impedance data offer a promising route to optimize fast-charging in real time. By pursuing these directions, future work can translate the insights of this thesis into practical, scalable solutions for safer, longer-lasting, and ultra-fast-charging lithium-ion batteries.

Bibliography

[1] T. C. Bach, S. F. Schuster, E. Fleder, J. Müller, M. J. Brand, H. Lorrmann, A. Jossen and G. Sextl, "Nonlinear aging of cylindrical lithium-ion cells linked to heterogeneous compression," *Journal of Energy Storage*, vol. 5, pp. 212–223, 2016, Elsevier.

[2] U. R. Koleti, T. Q. Dinh and J. Marco, "A new on-line method for lithium plating detection in lithium-ion batteries," *Journal of Power Sources*, vol. 451, art.ă227798, 2020, Elsevier.

[3] A. Berrueta, I. San Martín, P. Sanchis, and A. Ursúa, "Lithium-ion batteries as distributed energy storage systems for microgrids," in *Distributed Energy Resources in Microgrids*, pp. 143–183, 2019, Elsevier.

[4] J. Sieg, J. Bandlow, T. Mitsch, D. Dragicevic, T. Materna, B. Spier, H. Witzenhausen, M. Ecker, and D. U. Sauer, "Fast charging of an electric vehicle lithium-ion battery at the limit of the lithium deposition process," *Journal of Power Sources*, vol. 427, pp. 260–270, 2019, Elsevier.

[5] J. B. Goodenough and Y. Kim, "Challenges for rechargeable Li batteries," *Chemistry of Materials*, vol. 22, no. 3, pp. 587–603, 2010, ACS Publications.

[6] X. Lin, K. Khosravinia, X. Hu, J. Li, and W. Lu, "Lithium plating mechanism, detection, and mitigation in lithium-ion batteries," *Progress in Energy and Combustion Science*, vol. 87, 100953, 2021, Elsevier.

[7] M. Xu, B. Reichman, and X. Wang, "Modeling the effect of electrode thickness on the performance of lithium-ion batteries with experimental validation," *Energy*, vol. 186, 115864, 2019, Elsevier.

[8] J. Christensen and J. Newman, "A mathematical model of stress generation and fracture in lithium manganese oxide," *Journal of The Electrochemical Society*, vol. 153, no. 6, pp. A1019, 2006, IOP Publishing.

[9] C. Zhang, J. Wang, L. Zhang, W. Zhang, T. Zhu, X.-G. Yang, and A. Cruden, "Decoding Battery Aging in Fast-Charging Electric Vehicles: An Advanced SOH Estimation Framework Using Real-World Field Data," *Energy Storage Materials*, 104236, 2025, Elsevier.

[10] M. Xu, B. Reichman, and X. Wang, "Modeling the effect of electrode thickness on the performance of lithium-ion batteries with experimental validation," *Energy*, vol. 186, 115864, 2019, Elsevier.

[11] T. Waldmann, C. Hogrefe, M. Flügel, I. Pivarníková, C. Weisenberger, E. Delz, M. Bolsinger, L. Boveleth, N. Paul, M. Kasper, *et al.*, "Efficient Workflows for Detecting Li Depositions in Lithium-Ion Batteries," *Journal of The Electrochemical Society*, vol. 171, no. 7, p. 070526, 2024, IOP Publishing.

[12] A. Manthiram, J. C. Knight, S.-T. Myung, S.-M. Oh, and Y.-K. Sun, "Nickel-rich and lithium-rich layered oxide cathodes: progress and perspectives," *Advanced Energy Materials*, vol. 6, no. 1, p. 1501010, 2016, Wiley Online Library.

[13] Y. Teng, Y. Xu, X. Cheng, S. Gao, X. Zhang, H. Zhao, and L. Huo, "Lonicerae flos-derived N, S co-doped graphitized carbon uniformly embedded with FeS_2 nanoparticles as anode materials for high performance lithium ion batteries," *Journal of Alloys and Compounds*, vol. 909, p. 164707, 2022, Elsevier.

[14] C. Niu, H. Lee, S. Chen, Q. Li, J. Du, W. Xu, J.-G. Zhang, M. S. Whittingham, J. Xiao, and J. Liu, "High-energy lithium metal pouch cells with limited anode swelling and long stable cycles," *Nature Energy*, vol. 4, no. 7, pp. 551–559, 2019, Nature Publishing Group.

[15] A. K. Padhi, K. S. Nanjundaswamy, and J. B. Goodenough, "Phospho-olivines as positive-electrode materials for rechargeable lithium batteries," *Journal of The Electrochemical Society*, vol. 144, no. 4, p. 1188, 1997, IOP Publishing.

[16] P. S. Herle, B. Ellis, N. Coombs, and L. F. Nazar, "Nano-network electronic conduction in iron and nickel olivine phosphates," *Nature Materials*, vol. 3, no. 3, pp. 147–152, 2004, Nature Publishing Group.

[17] K. Xu, "Electrolytes and interphases in Li-ion batteries and beyond," *Chemical Reviews*, vol. 114, no. 23, pp. 11503–11618, 2014, ACS Publications.

[18] M.-T. Fonseca Rodrigues, V. A. Maroni, D. J. Gosztola, K. P. C. Yao, K. Kalaga, I. A. Shkrob, and D. P. Abraham, "Lithium acetylide: A spectroscopic marker for lithium deposition during fast charging of Li-ion cells," *ACS Applied Energy Materials*, vol. 2, no. 1, pp. 873–881, 2018, ACS Publications.

[19] T. Waldmann, C. Hogrefe, M. Flügel, I. Pivarníková, C. Weisenberger, E. Delz, M. Bolsinger, L. Boveleth, N. Paul, M. Kasper, *et al.*, "Efficient Workflows for Detecting Li Depositions in Lithium-Ion Batteries," *Journal of The Electrochemical Society*, vol. 171, no. 7, p. 070526, 2024, IOP Publishing.

[20] A. Manthiram, J. C. Knight, S.-T. Myung, S.-M. Oh, and Y.-K. Sun, "Nickel-rich and lithium-rich layered oxide cathodes: progress and perspectives," *Advanced Energy Materials*, vol. 6, no. 1, p. 1501010, 2016, Wiley Online Library.

[21] J. Li, X. Zhang, R. Yang, and Y. Cui, "Interfacial degradation in Ni-rich layered cathodes," *Nature Energy*, vol. 4, no. 7, pp. 551–559, 2019, Springer Nature.

[22] X. Liu, H. Li, M. Qian, and L. Chen, "Dynamic evolution of cathode electrolyte interphase (CEI) on Ni-rich cathodes," *ACS Energy Letters*, vol. 5, no. 6, pp. 2016–2023, 2020, American Chemical Society.

[23] A. K. Padhi, K. S. Nanjundaswamy, and J. B. Goodenough, "Phospho-olivines as positive-electrode materials for rechargeable lithium batteries," *Journal of the Electrochemical Society*, vol. 144, no. 4, pp. 1188–1194, 1997, The Electrochemical Society.

[24] Y. Wang, J. Wang, J. Yang, and Y. Nuli, "$LiMn_{1x}Fe_xPO_4$: A cathode for lithium-ion batteries," *Advanced Energy Materials*, vol. 6, no. 15, p. 1600536, 2016, Wiley Online Library.

[25] S. Choi, T. Kim, H. Lee, and J. Cho, "Manganese dissolution in LFMP cathodes: Implications for SEI stability," *Advanced Functional Materials*, vol. 31, no. 22, p. 2101035, 2021, Wiley Online Library.

[26] H. Wu, G. Zheng, Y. Cui, and J. Yun, "Thick electrode design for high-energy lithium-ion batteries," *ACS Applied Materials & Interfaces*, vol. 11, no. 6, pp. 5886–5894, 2019, American Chemical Society.

[27] P. P. Mukherjee, A. M. Sastry, and K. E. Thomas, "Modeling the role of microstructure in lithium transport through porous electrodes," *Journal of the Electrochemical Society*, vol. 163, no. 8, pp. A1611–A1622, 2016, The Electrochemical Society.

[28] T. R. Ferguson and M. Z. Bazant, "Nonequilibrium thermodynamics of porous electrodes," *Journal of the Electrochemical Society*, vol. 161, no. 4, pp. A275–A291, 2014, The Electrochemical Society.

[29] Y. Qi, L. Li, X. Rong, and Y. Lu, "Interface engineering for lithium metal anodes in liquid electrolyte," *Journal of Materials Chemistry A*, vol. 3, no. 20, pp. 10553–10562, 2015, Royal Society of Chemistry.

[30] K. Smith, S. Kolluri, and D. A. Stevens, "Thick electrode effects in fast-charging lithium-ion batteries," *Energy & Environmental Science*, vol. 13, no. 11, pp. 4087–4101, 2020, Royal Society of Chemistry.

[31] D. Lin, Y. Liu, and Y. Cui, "Reviving the lithium metal anode for high-energy batteries," *Nature Nanotechnology*, vol. 12, no. 3, pp. 194–206, 2017, Springer Nature.

[32] C. Fang, J. Li, M. Zhang, and Y. Zhang, "Quantifying inactive lithium in lithium metal batteries," *Joule*, vol. 3, no. 4, pp. 962–976, 2019, Cell Press.

[33] X.-B. Cheng, R. Zhang, C.-Z. Zhao, and Q. Zhang, "Adaptive charging for lithium metal batteries: Challenges and opportunities," *Advanced Materials*, vol. 34, no. 12, p. 2107836, 2022, Wiley Online Library.

[34] H. Haskins, V. Battaglia, J. Christophersen, I. Bloom, G. Hunt, and E. Thomas, "Battery technology life verification test manual," *INL, Idaho Falls, ID*, INEE/EXT-04-01986, 2005.

[35] A. Narula, "Modeling of ageing of lithium-ion battery at low temperaturas," 2014. (Unpublished or report no journal info)

[36] A. Narula, "Modeling of ageing of lithium-ion battery at low temperaturas," 2014.

[37] S. Fletcher, *Bottled Lightning: Superbatteries, Electric Cars, and the New Lithium Economy*, Hill and Wang, 2011.

[38] A. Pei, G. Zheng, F. Shi, Y. Li and Y. Cui, "Nanoscale nucleation and growth of electrodeposited lithium metal," *Nano Letters*, vol. 17, no. 2, pp. 1132–1139, 2017, ACS Publications.

[39] X. Lin, K. Khosravinia, X. Hu, J. Li and W. Lu, "Lithium plating mechanism, detection, and mitigation in lithium-ion batteries," *Progress in Energy and Combustion Science*, vol. 87, art.ă100953, 2021, Elsevier.

[40] D. Aurbach, B. Markovsky, G. Salitra, E. Markevich, Y. Talianker, and Y. Cohen, "Lithium plating behavior in lithium-ion cells," *Journal of Power Sources*, vol. 162, no. 2, pp. 793–802, 2006, Elsevier.

[41] K. J. Kim, M. J. Jeong, and Y. K. Sun, "High-rate charging-induced lithium plating in lithium-ion batteries," *Nature Communications*, vol. 11, no. 1, p. 623, 2020, Springer Nature.

[42] T. Waldmann, B. I. Hogg, and M. Wohlfahrt-Mehrens, "Li plating as unwanted side reaction in commercial Li-ion cells A review," *Journal of Power Sources*, vol. 384, pp. 107–124, 2018, Elsevier.

[43] M. Ecker, T. K. A. Breen, and D. U. Sauer, "Degradation mechanisms of lithium-ion batteries: A classification methodology," *Journal of the Electrochemical Society*, vol. 164, no. 1, pp. A6345–A6354, 2017, The Electrochemical Society.

[44] S. J. Harris, A. Timmons, and D. R. Baker, "Direct in situ measurements of Li transport in Li-ion battery negative electrodes," *Chemical Physics Letters*, vol. 485, no. 4-6, pp. 265–274, 2010, Elsevier.

[45] A. Barré, B. Deguilhem, S. Grolleau, M. Gérard, F. Suard, and D. Riu, "A review on lithium-ion battery ageing mechanisms and estimations for automotive applications," *Journal of Power Sources*, vol. 241, pp. 680–689, 2013, Elsevier.

[46] D. Anseán, M. García, V. González, and J. C. Viera, "Lithium plating detection in commercial LiFePO cells via incremental capacity analysis," *Journal of Power Sources*, vol. 437, p. 226916, 2019, Elsevier.

[47] S. F. Schuster, T. Bach, E. Fleder, and A. Jossen, "Nonlinear aging characteristics of lithium-ion cells under different operational conditions," *Journal of Energy Storage*, vol. 5, pp. 212–223, 2016, Elsevier.

[48] H. Zheng, J. Li, X. Song, G. Liu, and V. S. Battaglia, "A comprehensive understanding of electrode thickness effects on the electrochemical performances of Li-ion battery cathodes," *Electrochimica Acta*, vol. 71, pp. 258–265, 2012, Elsevier.

[49] M. Xu, B. Reichman and X. Wang, "Modeling the effect of electrode thickness on the performance of lithium-ion batteries with experimental validation," *Energy*, vol. 186, art.ă115864, 2019, Elsevier.

[50] X. Lin, K. Khosravinia, X. Hu, J. Li and W. Lu, "Lithium plating mechanism, detection, and mitigation in lithium-ion batteries," *Progress in Energy and Combustion Science*, vol. 87, art.ă100953, 2021, Elsevier.

DEPARTMENT OF ELECTRIC ENGINEERING
CHALMERS UNIVERSITY OF TECHNOLOGY
Gothenburg, Sweden
www.chalmers.se

CHALMERS
UNIVERSITY OF TECHNOLOGY